doi:10.1093/brain/aww163 BRAIN 2016: 139; 2372–2379 | 2372

BRAIN
A JOURNAL OF NEUROLOGY

REPORT

^{18}F-AV-1451 tau PET imaging correlates strongly with tau neuropathology in *MAPT* mutation carriers

Ruben Smith,[1,2] Andreas Puschmann,[1,2] Michael Schöll,[3,4] Tomas Ohlsson,[5] John van Swieten,[6] Michael Honer,[7] Elisabet Englund[8] and Oskar Hansson[3,9]

Tau positron emission tomography ligands provide the novel possibility to image tau pathology *in vivo*. However, little is known about how *in vivo* brain uptake of tau positron emission tomography ligands relates to tau aggregates observed post-mortem. We performed tau positron emission tomography imaging with ^{18}F-AV-1451 in three patients harbouring a p.R406W mutation in the *MAPT* gene, encoding tau. This mutation results in 3- and 4-repeat tau aggregates similar to those in Alzheimer's disease, and many of the mutation carriers initially suffer from memory impairment and temporal lobe atrophy. Two patients with short disease duration and isolated memory impairment exhibited ^{18}F-AV-1451 uptake mainly in the hippocampus and adjacent temporal lobe regions, correlating with glucose hypometabolism in corresponding regions. One patient died after 26 years of disease duration with dementia and behavioural deficits. Pre-mortem, there was ^{18}F-AV-1451 uptake in the temporal and frontal lobes, as well as in the basal ganglia, which strongly correlated with the regional extent and amount of tau pathology in post-mortem brain sections. Amyloid-β (^{18}F-flutemetamol) positron emission tomography scans were negative in all cases, as were stainings of brain sections for amyloid. This provides strong evidence that ^{18}F-AV-1451 positron emission tomography can be used to accurately quantify *in vivo* the regional distribution of hyperphosphorylated tau protein.

1 Department of Clinical Sciences Lund, Department of Neurology, Lund University, Sweden
2 Department of Neurology and Rehabilitation Medicine, Skåne University Hospital, Lund, Sweden
3 Clinical Memory Research Unit, Department of Clinical Sciences Malmö, Lund University, Sweden
4 MedTech West and the Division of Clinical Neuroscience, Gothenburg University, Gothenburg, Sweden
5 Department of Radiation physics, Skåne University Hospital, Lund, Sweden
6 Department of Neurology, Erasmus Medical Centre, Rotterdam, The Netherlands
7 Roche Pharmaceutical Research and Early Development, Neuroscience Discovery and Biomarkers, Roche Innovation Center, Basel, Switzerland
8 Division of Oncology and Pathology, Department of Clinical Sciences, Lund University, Sweden
9 Memory Clinic, Skåne University Hospital, Malmö, Sweden

Correspondence to: Ruben Smith,
Department of Neurology, Skåne University Hospital,
Lund, SE-20502,
Sweden
E-mail: Ruben.Smith@med.lu.se

Correspondence may also be addressed to: Oskar Hansson, Memory Clinic, Skåne University Hospital, Malmö, SE-20502, Sweden
E-mail: oskar.hansson@med.lu.se

Keywords: tau; frontotemporal dementia; Alzheimer's disease; positron emission tomography; MAPT R406W mutation

Abbreviations: FDG = fluorodeoxyglucose; PHF = paired helical filaments; SUVR = standardized uptake value ratio

Received March 2, 2016. Revised May 22, 2016. Accepted May 27, 2016. Advance Access publication June 29, 2016

Introduction

Tau pathology is closely related to neuronal dysfunction and degeneration in Alzheimer's disease and other tauopathies. In these disorders, tau is abnormally hyperphosphorylated and accumulates intracellularly, forming tangles of paired helical filaments (PHF), twisted ribbons and/or straight filaments (Iqbal *et al.*, 2016). Tau aggregates in Alzheimer's disease consist predominantly of PHF, which contain all six isoforms of tau, mixed with straight filaments. The recent development of PET radiotracers for tau aggregates opens up the possibility to assess tau pathology *in vivo* (Ossenkoppele *et al.*, 2015; Villemagne and Okamura, 2015; Harada *et al.*, 2016; Johnson *et al.*, 2016; Scholl *et al.*, 2016; Smith *et al.*, 2016). These tracers, along with PET tracers revealing extracellular plaques containing amyloid-β fibrils, will be essential for improving the early diagnosis of Alzheimer's disease in clinical practice as well as in the evaluation of novel disease-modifying therapies (Dani *et al.*, 2016).

Studies using the most common PET tracer for tau pathology to date, ^{18}F-AV-1451, demonstrated increased uptake in temporo-parietal regions in patients with Alzheimer's disease (Chien *et al.*, 2013; Johnson *et al.*, 2016; Ossenkoppele *et al.*, 2016; Smith *et al.*, 2016). In post-mortem brain tissue, this ligand was screened to detect PHFs of tau, exhibiting a >25-fold higher affinity for PHF-tau compared to amyloid-β fibrils (Xia *et al.*, 2013). Recently, an autoradiography study reported preferential *in vitro* binding of ^{18}F-AV-1451 to PHFs in Alzheimer's disease, not to straight filaments resulting from other tauopathies (Marquie *et al.*, 2015). However, no study has hitherto compared regional *in vivo* binding of a tau PET tracer with the distribution and the degree of tau pathology using post-mortem immunohistochemistry in the same individual.

Individuals exhibiting only tau pathology, not amyloid-β fibrils, are an ideal group to further explore the binding properties of a tau PET tracer. The p.R406W mutation in the gene encoding the tau protein (*MAPT* c.1216C>T; R406W) on chromosome 17 results in neurofibrillary tangles that are similar to the neurofibrillary tangles in Alzheimer's disease at an ultrastructural level (Ghetti *et al.*, 2015). Many cases with this mutation present with slowly progressive episodic memory impairment, which in many ways clinically resembles Alzheimer's disease (Ostojic *et al.*, 2004; Passant *et al.*, 2004). Previous neuropathological examination of R406W mutation carriers revealed tau-positive neurofibrillary tangles and neurites. These PHF-tau changes were mainly localized in temporal and frontal lobe areas as well as the basal ganglia, sparing the parietal and occipital lobes (Lindquist *et al.*, 2008; Ghetti et al., 2015).

Here we report the first results of ^{18}F-AV-1451 (tau), ^{18}F-flutemetamol (amyloid-β) and ^{18}F-fluorodeoxyglucose (FDG, glucose metabolism) PET imaging in three patients carrying the MAPT R406W mutation at different disease stages. In addition, we report results from the neuropathological examination of one of these subjects who died 2 weeks after the PET scans, as well as the relationship between *in vivo* and post-mortem assessment of tau pathology in this case. Finally, autoradiography using ^{3}H-AV1451 was performed on cortical tissue sections from two additional deceased patients with the MAPT R406W mutation.

Materials and methods

Participants

Three subjects carrying the MAPT R406W mutation, aged 56, 60 and 76 years, (Patients A, B and C, respectively) from a family with hereditary dementia from Southern Sweden were investigated. Four control subjects and five patients with Alzheimer's disease were recruited from the ongoing Swedish Biofinder Study (www.biofinder.se). Further information on the clinical assessments is given in the Supplementary material. All clinical data are summarized in Table 1. Written informed consent was obtained from the participants, and approval of this study was obtained from the Regional Ethical Review Board in Lund, Sweden.

MRI and CT scan

Patients A and B underwent a 3 T MRI scan using a Siemens Skyra scanner. T_1-weighted magnetization-prepared rapid gradient echo (T_1-MPRAGE) was acquired at a resolution of $1 \times 1 \times 1$ mm. Patient C could not undergo MRI due to claustrophobia and consequently underwent a CT scan, using a Philips Brilliance 64 scanner. Images were reconstructed to 5 mm axial and 3 mm coronal slices.

PET

^{18}F-AV-1451 PET scans were performed on a GE Discovery 690 PET scanner (General Electric Medical Systems) as dynamic scans using LIST-mode 100–120 min after a bolus injection of 365 ± 14 MBq of ^{18}F-AV-1451. ^{18}F-FDG scans were acquired on the same scanner in a static scan 60–80 min after injection of 198 ± 2 MBq of FDG. Images of ^{18}F-flutemetamol (Nelissen *et al.*, 2009) were obtained as dynamic scans 90–110 min after injection of 193 ± 2 MBq on a Philips Gemini TF PET-CT scanner (Philips Medical Systems). Low dose CT scans for attenuation correction were performed immediately prior to the PET scans. PET data were reconstructed into 5 min frames using an iterative Vue Point HD algorithm with six subsets, 18 iterations with 3 mm filter and no time-of-flight correction. ^{18}F-flutemetamol data were processed using NeuroMarQ software (GE Healthcare), analyses of ^{18}F-AV-1451 and ^{18}F-FDG data were performed using PMOD 3.603 software (Pmod, Zurich, Switzerland). PET images were co-registered to their corresponding magnetic resonance T_1-MPRAGE or CT images. We chose to analyse the ^{18}F-AV-1451 standardized uptake value ratios (SUVRs) from the same areas that were processed for neuropathological analysis in Patient C, with the addition of a few areas in the

Table 1 Clinical characteristics of study participants

	Case A	Case B	Case C	Controls ($n = 4$)
Age at examination (years)	60	56	76	71.5 ± 7
Gender	M	F	F	2M / 2F
Disease duration (years)	10	4	26	N/A
Genotype	*MAPT* c.1216C>T (het)	*MAPT* c.1216C>T (het)	*MAPT* c.1216C>T (het)	N/A
MMSE	26	24	N/T	28.75 ± 1.5
Memory delayed recall (ADAS)	8	10	N/T	1.25 ± 1
AQT (s)	57	68	N/T	61 ± 13
SDMT	32	42	N/T	37 ± 10
Stroop (s)	18	24	N/T	19 ± 3
TMT-A (s)	55	49	N/T	37 ± 12
Letter S-fluency	25	14	N/T	15 ± 6
Animal fluency	26	20	N/T	24 ± 5

ADAS 3 = Alzheimer's Disease Assessment Acale, part 3; AQT (C + S = Colour + Shape) = A Quick Test of Cognitive Speed; MMSE = Mini-Mental State Examination; N/A = not available; N/T = unable to complete testing; SDMT = Symbol Digit Modalities Test; Stroop = Stroop Color-Word Test; TMT-A = Trail Making Test, part A.
For all tests except ADAS, AQT, Stroop and TMT, a lower value reflects higher degree of cognitive dysfunction.

temporal and frontal lobes and the basal ganglia, areas known to be affected by pathology in R406W mutation carriers. Regions of interest were delineated manually for the data presented in Figs 1 and 3. Regions of interest were delineated on the magnetic resonance images (Patients A and B, as well as control subjects and cases with Alzheimer's disease) or CT image (Patient C) and transformed into PET space using transformations derived from co-registrations. The cerebellar cortex was used as a reference region for the calculation of SUVRs.

For the analysis of correlations between regional ^{18}F-FDG SUVRs and ^{18}F-AV-1451 SUVRs in Patients A and B (Fig. 2), the MRI was segmented into grey and white matter and regions of interest were defined using FreeSurfer (version 5.3 and its Desikan-Killiany Atlas). PET images were co-registered to the MRIs and SUVRs calculated in PET space. The cerebellar cortex was also here used as a reference region for the calculation of SUVRs. Further, the SUVRs of the ^{18}F-FDG scans were normalized to the mean control ^{18}F-FDG value for each neocortical region in order to relate the tau pathology to the relative change of the ^{18}F-FDG uptake in Patients A and B, respectively (Smith *et al.*, 2016).

Neuropathology

Neuropathological diagnostic analysis was performed on sections including the hippocampus, the inferior and superior temporal gyri, the frontal pole and the dorsolateral frontal gyri, the parietal cortex, occipital cortex and cerebellum. Details of immunohistochemical procedures are described in the Supplementary material. Neurodegenerative structural changes were assessed as to regional extent, local–regional severity and to intensity/density of protein pathology, with regard to tau appearance. Tau pathology in the cortical compartment was readily graded in none, mild, moderate, and severe (grades 0, +, + + and + + +, respectively), for correlation with ^{18}F-AV-1451 uptake. Mild grade (+) corresponded with few loosely knit aggregates of tau-positive fibres in one or two cortical layers, mostly the laminae II–III, and a few dispersed tau-positive neurites between the aggregates. Moderate grade (+ +) signified scattered loosely knit fibre aggregates in all layers, with tau-positive scattered neurites and occasional tangle-filled neurons in-between. In severe grade (+ + +), abundant aggregates were seen in all layers, with numerous tau-positive neurites and several tau-positive tangle-filled neurons in-between. Inter-rater reliability was determined by three independent, blinded readers (Cohen's kappa, 0.72–0.84; $P < 0.001$; SPSS version 22). As a second independent measure of tau-positive neurite density, the number of neurites/μm was estimated in the cortex of tau-stained sections using stereological systematic random sampling (Ronn *et al.*, 2000) (Stereo Investigator, MBF Bioscience). Only cortical areas and the putamen could be reliably sampled using this stereological approach.

Autoradiography

Details of the methods regarding autoradiography are described in the Supplementary material.

Statistical analyses

Correlations between neurite density, the neuropathological grade of tau pathology and ^{18}F-AV-1451 SUVR values as well as the correlation between ^{18}F-FDG and ^{18}F-AV-1451 SUVR were analysed with non-parametric Spearman's Rank-Order Correlation using Graph Pad Prism 6. A *P*-value of < 0.05 was considered statistically significant.

Results

Study subjects

The three examined patients belonged to two generations of a family with slowly progressive dementia; all carried the MAPT R406W mutation. Cognitive testing of Patients A and B revealed an isolated memory impairment (Table 1), and both fulfilled the criteria of mild cognitive impairment (Petersen, 2004). Patient A had a 10-year history of isolated short-term memory loss and irritability and Patient B had developed mild memory impairment and increased anxiety

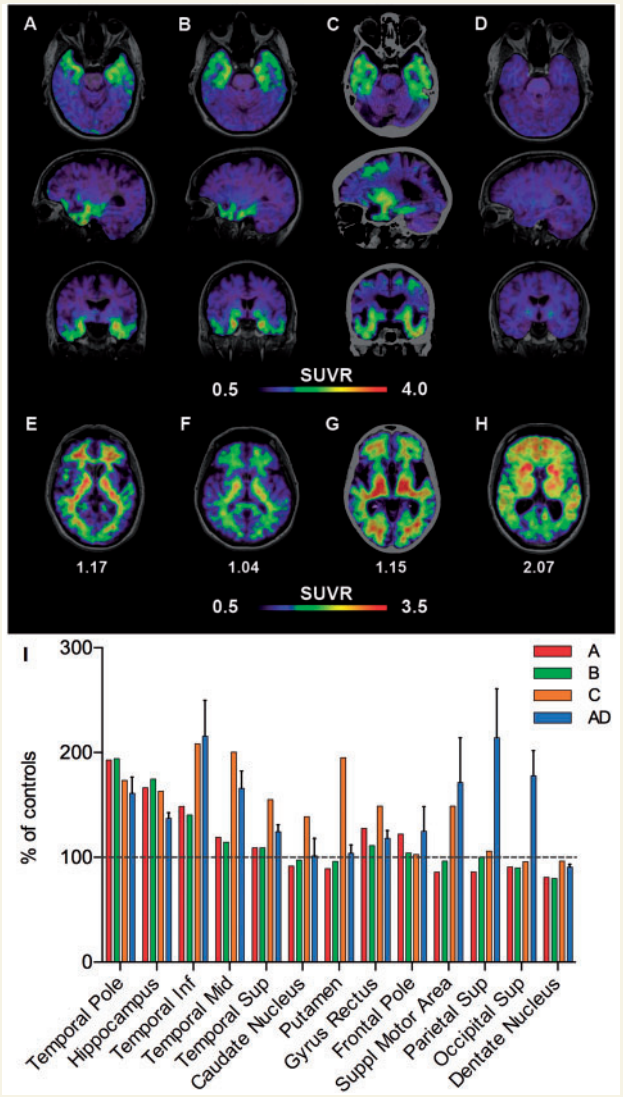

Figure 1 ^{18}F-AV-1451 and ^{18}F-flutemetamol PET. (**A–D**) ^{18}F-AV-1451 scans of tau mutation carriers A–C in panels **A–C**, respectively. A representative control subject is shown in **D**. (**E–H**) ^{18}F-flutemetamol PET. Patients **A–C** in panels **E–G**, respectively. (**H**) A positive scan typical for a patient with Alzheimer's disease. The signal in **A–C** represents non-specific white matter binding. Numbers below images indicate the composite score for global cortical mean uptake. (**I**) SUVRs, expressed as per cent of control values for (from *left* to *right* for each region) Patients A (red), B (green), C (orange), and Alzheimer's disease (AD) (blue). Patients with Alzheimer's disease are presented ± standard error of the mean.

4 years prior to the clinical examination. MRI in both cases showed no or slight general brain atrophy with moderate atrophy in the medial temporal lobes, most pronounced in the parahippocampal gyri with widening of the collateral sulci, and a medial temporal atrophy corresponded to Scheltens score 1. Patient C exhibited memory impairment 26 years prior to this examination and had developed marked dementia, behavioural disturbances, mutism, dysphagia and mild parkinsonism by the time of this study. The CT scan showed generalized cortical atrophy with substantial atrophy of the medial temporal lobes, especially of the parahippocampal gyri with pronounced widening of the collateral sulci. Medial temporal atrophy corresponded to Scheltens score 3.

^{18}F-AV-1451 and ^{18}F-flutemetamol PET

In the two younger cases (Patients A and B; Fig. 1A, B and I), retention of ^{18}F-AV-1451 was most distinct in the temporal poles, the hippocampus and anterior aspects of the inferior temporal gyrus. Uptake was also detected in the basal regions of the frontal lobes. In the more affected case (Patient C, Fig. 1C and I), a more widespread retention pattern was observed in the temporal lobes, the basal ganglia and the frontal lobes. No significant tracer uptake was detected in the parietal or occipital lobes. Control cases showed no tracer retention in cortical areas (Fig. 1D and Supplementary Fig. 1).

The patients further underwent ^{18}F-flutemetamol PET scans. Composite scores representing mean global cortical uptake were below a previously determined cut-off for amyloid-β-positivity (<1.42; Palmqvist *et al.*, 2014) in the three patients who did not show visual signs of cortical ^{18}F-flutemetamol retention either (Fig. 1E–G).

Correlation of ^{18}F-AV-1451 with ^{18}F-FDG

Patients A and B underwent an additional ^{18}F-FDG scan. The ^{18}F-FDG SUVRs for each region were normalized to the controls' regional SUVRs and correlated with the corresponding AV-1451 SUVRs (Fig. 2A–D). We found statistically significant inverse relationships of higher regional AV-1451 uptake with lower FDG retention in both patients (Patient A: $r_s = -0.39$, $P < 0.01$, Fig. 2E; Patient B: $r_s = -0.37$, $P < 0.01$, Fig. 2F).

Neuropathology

Patient C died 2 weeks after the PET examinations. Immunohistochemical staining for hyperphosphorylated tau protein showed extensive neuronal tau pathology in the temporo-limbic region, the anterior temporal lobe and hippocampus, where tau-positive neurofibrillary tangles were abundant along with tau-positive neurites. Lower-grade pathology was detected in frontal cortical areas, whereas posterior cortical areas were only affected to a minor degree. Tau pathology was assessed according to a four-point grading system (0, +, + +, + + +), as described above, and results are summarized in Fig. 3A–J. Both 3R and 4R tau-positive neurites could be detected using isotype specific antibodies (data not shown). No amyloid-β-containing neuritic plaques or amyloid angiopathy were detected (data not shown).

Non-parametric correlation analysis showed a statistically highly significant positive correlation between

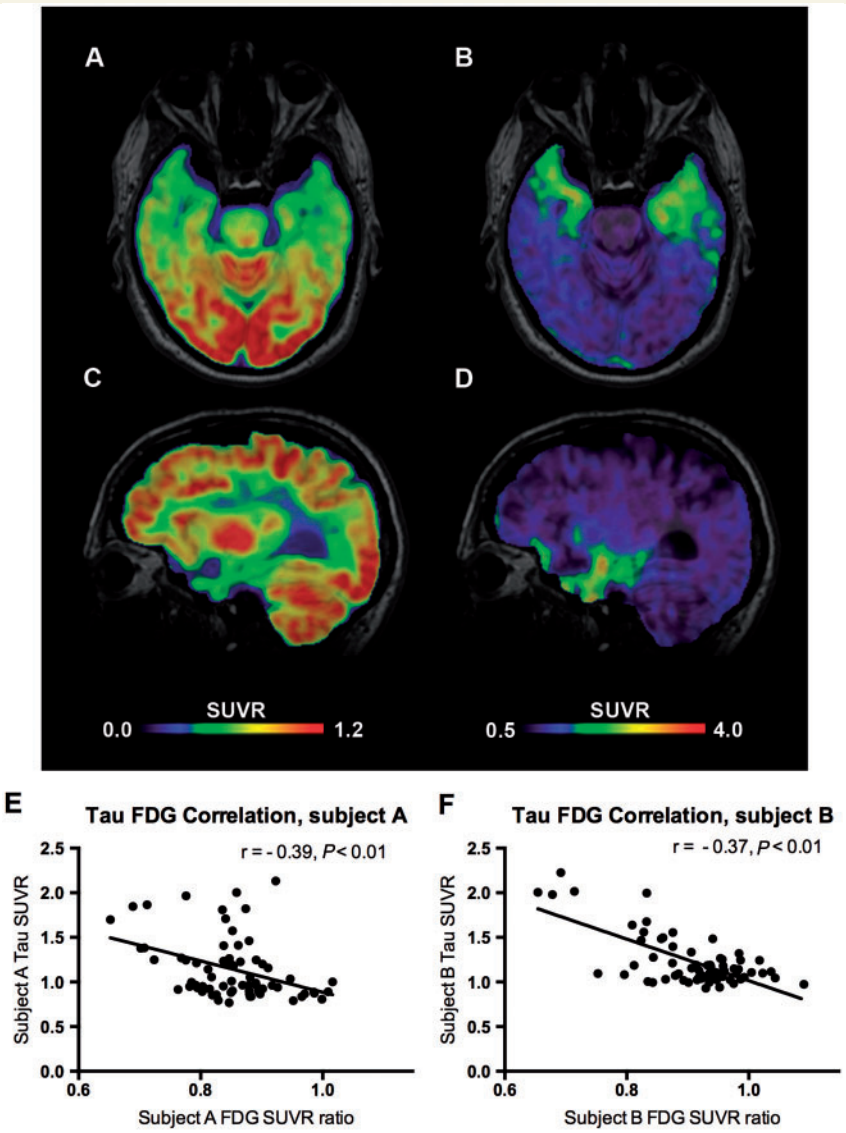

Figure 2 Correlation of ^{18}F-FDG with ^{18}F-AV-1451. (**A–D**) Images of Patient A. (**A** and **C**) Transverse and sagittal images of ^{18}F-FDG, scale showing range of SUVR values. (**B** and **D**) Transverse and sagittal images of ^{18}F-AV-1451, scale showing range of SUVR values. (**E** and **F**) Correlation between FDG and AV-1451 in Patients A (**E**) and B (**F**). Patient FDG-SUVRs have been normalized to control FDG-SUVR values for each region. Line represents a linear regression.

^{18}F-AV-1451 SUVRs in different brain regions and the severity of tau-neuropathology according to immunohistochemistry in the same regions when using either neuropathological grading of tau pathology ($r = 0.93$, $P < 0.01$; Fig. 3I) or quantification of the density of tau-positive neurites ($r = 0.92$, $P < 0.01$; Fig. 3K). Interestingly, the region with the highest SUVR (2.85) was putamen, which did not exhibit higher tau pathology density than the inferior temporal lobe with an SUVR of 2.38.

Autoradiography

Cortical tissue samples from two other patients with the R406W MAPT mutation were analysed using autoradiography. Specific binding of ^{3}H-AV1451 to tau aggregates could be detected in the cortical tissue sections of both patients. Radioligand binding was co-localized with tau aggregates, as visualized by immunohistochemistry with the tau-specific antibody AT8 (Supplementary Fig. 2).

Discussion

In the present study we describe three members of a family with MAPT R406W mutation at different stages of a degenerative neurological disorder. *In vivo* imaging with ^{18}F-AV-1451 PET indicated that tau pathology in these cases starts in the inferior temporal lobes and temporal poles, and at a later stage also involves the basal ganglia and the frontal cortex while sparing posterior cortical areas

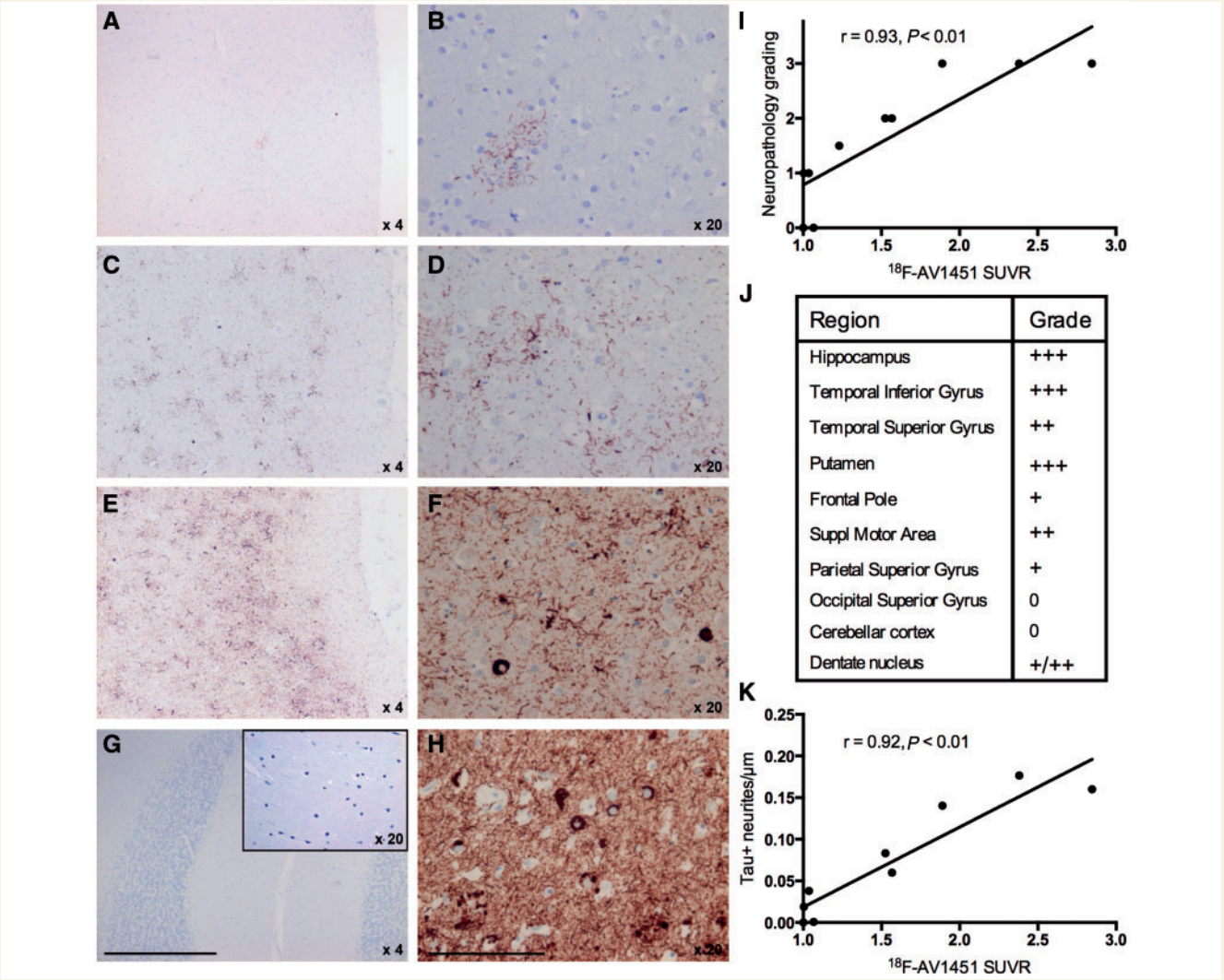

Figure 3 ^{18}F-AV-1451 correlation with neuropathology. (**A** and **B**) Tau inclusions, grade +, at ×4 (**A**) and ×20 magnification (**B**). (**C** and **D**) Grade + +, at ×4 (**C**) and ×20 magnification (**D**). Grade + + +, at ×4 (**E**) and ×20 magnification (**F**). (**G**) Cerebellar white matter and cortex (grade 0) at ×4 magnification. Inset at ×20 magnification. (**H**) Positive control, cortex from a patient with Alzheimer's disease at ×20 magnification. Scale bars = 500 µm at ×4 and 100 µm at ×20 magnifications. (**I**) Correlation between ^{18}F-AV-1451 and neuropathological grade. Line represents a linear regression. Spearman correlation: $r_s = 0.93$, $P < 0.01$. (**J**) Neuropathological grades in the brain regions analysed. (**K**) Correlation of tau-positive neurite density and ^{18}F-AV-1451 SUVR in the cortical regions analysed and the putamen. Line represents a linear regression. Spearman correlation: $r_s = 0.92$, $P < 0.01$.

and the cerebellum. In one patient who died shortly after PET scanning and was examined neuropathologically, we found a strong positive correlation between the regional *in vivo* retention of ^{18}F-AV-1451 and the density of tau aggregates visualized with immunohistochemistry in post-mortem brain tissue. Our study is the first to report ^{18}F-AV-1451 PET signal being directly correlated to neuropathological tau burden in the same individual, which provides strong evidence that *in vivo* ^{18}F-AV-1451 PET retention indeed reflects the density of tau pathology consisting of PHFs. However, it is known that unspecific retention of ^{18}F-AV-1451 occurs in the striatum and choroid plexus, for example (Scholl *et al.*, 2016). It is therefore interesting to note that the region with highest retention of ^{18}F-AV-1451 in Patient C was the putamen. The neuropathological evaluation revealed relatively severe tau pathology in this region, but even greater pathological burden was observed in the inferior temporal lobe, which exhibited a slightly lower retention of ^{18}F-AV-1451 (Fig. 3K), indicating that a proportion of the signal in the putamen might represent unspecific tracer retention in addition to the specific binding to tau aggregates.

The R406W mutation is located in the N-terminal exon 13 of the *MAPT* gene and causes the formation of agglomerations containing six isoforms of tau (including 3R and 4R tau) highly similar to the aggregates found in Alzheimer's disease (Hong *et al.*, 1998; Ghetti *et al.*, 2015), which was corroborated in the present study.

At an ultrastructural level the tau filaments are PHF and straight filaments with a diameter of 8–20 nm, structurally similar to filaments found in Alzheimer's disease (Reed *et al.*, 1997; Hutton *et al.*, 1998). It has previously been shown that ^{18}F-AV-1451 can detect tau aggregates in patients with Alzheimer's disease (Ossenkoppele *et al.*, 2015; Johnson *et al.*, 2016; Smith *et al.*, 2016). Our study provides proof of concept that it is also possible to visualize tau pathology in R406W tau mutation carriers using ^{18}F-AV-1451 PET. This is in accordance with a recent study reporting highly concordant patterns of staining with tau-antibody AT8 and ^{18}F-AV-1451 binding in post-mortem brain tissue of among others, Alzheimer's disease patients and subjects carrying *MAPT* mutations (Sander *et al.*, 2016), although this study also found evidence for off-target binding and lack of correlation between antibody staining and *in vitro* tracer binding in certain tau strains. However, the present study indicates that the *in vivo* binding of ^{18}F-AV-1451 correlates highly with the extent of tau aggregates containing PHF. With tau immunization therapies for Alzheimer's disease currently emerging (Pedersen and Sigurdsson, 2015), tau mutation carriers constitute the ideal population for studying the effects of these therapies. Not only would it be possible to examine the effects of anti-tau treatment in the absence of concurrent amyloid-β pathology, but also to identify and recruit subjects to clinical trials at a presymptomatic disease stage. Our results also suggest that one study endpoint in such clinical trials could be ^{18}F-AV-1451 retention.

Furthermore, we found an inverse relationship between the retention of ^{18}F-AV-1451 and brain glucose metabolism as measured by ^{18}F-FDG, indicative of decreased neuronal metabolism and dysfunction in areas affected by tau pathology. These results indicate that tau-pathology is tightly associated with neuronal dysfunction, which is in line with previous publications on tau and glucose hypometabolism in Alzheimer's disease (Ossenkoppele *et al.*, 2015; Smith *et al.*, 2016). Similarly, cognitive testing in Patients A and B only showed deficits restricted to memory, likely reflecting the limited distribution of tau pathology and glucose hypometabolism to the inferior and medial temporal lobes in these two cases.

In conclusion, our results strongly support the notion that *in vivo* ^{18}F-AV-1451 PET reflects the intensity of regional tau neuropathology. The level of ^{18}F-AV-1451 retention correlates with glucose hypometabolism and neuronal dysfunction. Tau pathology in R406W mutation carriers can be visualized using ^{18}F-AV-1451 PET, thus providing a useful tool for monitoring the effects of future therapies directed against the formation of tau-inclusions in these patients.

Acknowledgements

We wish to acknowledge the contribution of Dr Olof Strandberg, Dr Douglas Hägerström and Dr Jonas Jögi at Skåne University Hospital. The precursor of AV-1451 was provided by Avid Radiopharmaceuticals and [18F]-flutemetamol was by GE Healthcare, but no funding was received from the companies. The data were analysed and the manuscript written independent from any company interests.

Funding

The study was funded by the Swedish Research Council, the European Research Council, the Swedish Brain Foundation, the Swedish Alzheimer foundation, the Trolle-Wachtmeister Foundation and the Swedish Federal Government under the ALF Agreement.

Supplementary material

Supplementary material is available at *Brain* online.

References

Chien DT, Bahri S, Szardenings AK, Walsh JC, Mu F, Su MY, et al. Early clinical PET imaging results with the novel PHF-tau radioligand [F-18]-T807. J Alzheimers Dis 2013; 34: 457–68.

Dani M, Brooks DJ, Edison P. Tau imaging in neurodegenerative diseases. Eur J Nucl Med Mol Imaging 2016; 43: 1139–50.

Ghetti B, Oblak AL, Boeve BF, Johnson KA, Dickerson BC, Goedert M. Invited review: frontotemporal dementia caused by microtubule-associated protein tau gene (MAPT) mutations: a chameleon for neuropathology and neuroimaging. Neuropathol Appl Neurobiol 2015; 41: 24–46.

Harada R, Okamura N, Furumoto S, Furukawa K, Ishiki A, Tomita N, et al. 18F-THK5351: a novel PET radiotracer for imaging neurofibrillary pathology in Alzheimer disease. J Nucl Med 2016; 57: 208–14.

Hong M, Zhukareva V, Vogelsberg-Ragaglia V, Wszolek Z, Reed L, Miller BI, et al. Mutation-specific functional impairments in distinct tau isoforms of hereditary FTDP-17. Science 1998; 282: 1914–17.

Hutton M, Lendon CL, Rizzu P, Baker M, Froelich S, Houlden H, et al. Association of missense and 5'-splice-site mutations in tau with the inherited dementia FTDP-17. Nature 1998; 393: 702–5.

Iqbal K, Liu F, Gong CX. Tau and neurodegenerative disease: the story so far. Nat Rev Neurol 2016; 12: 15–27.

Johnson KA, Schultz A, Betensky RA, Becker JA, Sepulcre J, Rentz D, et al. Tau PET imaging in aging and early Alzheimer's disease. Ann Neurol 2016; 79: 110–9.

Lindquist SG, Holm IE, Schwartz M, Law I, Stokholm J, Batbayli M, et al. Alzheimer disease-like clinical phenotype in a family with FTDP-17 caused by a MAPT R406W mutation. Eur J Neurol 2008; 15: 377–85.

Marquie M, Normandin MD, Vanderburg CR, Costantino IM, Bien EA, Rycyna LG, et al. Validating novel tau positron emission tomography tracer [F-18]-AV-1451 (T807) on postmortem brain tissue. Ann Neurol 2015; 78: 787–800.

Nelissen N, Van Laere K, Thurfjell L, Owenius R, Vandenbulcke M, Koole M, et al. Phase 1 study of the Pittsburgh compound B derivative 18F-flutemetamol in healthy volunteers and patients with probable Alzheimer disease. J Nucl Med 2009; 50: 1251–9.

Ossenkoppele R, Schonhaut DR, Baker SL, O'Neil JP, Janabi M, Ghosh PM, et al. Tau, amyloid, and hypometabolism in a patient with posterior cortical atrophy. Ann Neurol 2015; 77: 338–42.

Ossenkoppele R, Schonhaut DR, Scholl M, Lockhart SN, Ayakta N, Baker SL, et al. Tau PET patterns mirror clinical and neuroanatomical variability in Alzheimer's disease. Brain 2016; 139: 1151–67.

Ostojic J, Elfgren C, Passant U, Nilsson K, Gustafson L, Lannfelt L, et al. The tau R406W mutation causes progressive presenile dementia with bitemporal atrophy. Dement Geriatr Cogn Disord 2004; 17: 298–301.

Palmqvist S, Zetterberg H, Blennow K, Vestberg S, Andreasson U, Brooks DJ, et al. Accuracy of brain amyloid detection in clinical practice using cerebrospinal fluid beta-amyloid 42: a cross-validation study against amyloid positron emission tomography. JAMA Neurol 2014; 71: 1282–9.

Passant U, Ostojic J, Froelich Fabre S, Gustafson L, Lannfelt L, Larsson EM, et al. Familial presenile dementia with bitemporal atrophy. Dement Geriatr Cogn Disord 2004; 17: 287–92.

Pedersen JT, Sigurdsson EM. Tau immunotherapy for Alzheimer's disease. Trends Mol Med 2015; 21: 394–402.

Petersen RC. Mild cognitive impairment as a diagnostic entity. J Intern Med 2004; 256: 183–94.

Reed LA, Grabowski TJ, Schmidt ML, Morris JC, Goate A, Solodkin A, et al. Autosomal dominant dementia with widespread neurofibrillary tangles. Ann Neurol 1997; 42: 564–72.

Ronn LC, Ralets I, Hartz BP, Bech M, Berezin A, Berezin V, et al. A simple procedure for quantification of neurite outgrowth based on stereological principles. J Neurosci Methods 2000; 100: 25–32.

Sander K, Lashley T, Gami P, Gendron T, Lythgoe MF, Rohrer JD, et al. Characterization of tau positron emission tomography tracer [F]AV-1451 binding to postmortem tissue in Alzheimer's disease, primary tauopathies, and other dementias. Alzheimers Dement 2016, doi: 10.1016/j.jalz.2016.01.003.

Scholl M, Lockhart SN, Schonhaut DR, O'Neil JP, Janabi M, Ossenkoppele R, et al. PET imaging of tau deposition in the aging human brain. Neuron 2016; 89: 971–82.

Smith R, Wibom M, Olsson T, Hagerstrom D, Jogi J, Rabinovici GD, et al. Posterior accumulation of tau and concordant hypometabolism in an early-onset Alzheimer's disease patient with presenilin-1 mutation. J Alzheimers Dis 2016; 51: 339–43.

Villemagne VL, Okamura N. Tau imaging in the study of ageing, Alzheimer's disease, and other neurodegenerative conditions. Curr Opin Neurobiol 2015; 36: 43–51.

Xia CF, Arteaga J, Chen G, Gangadharmath U, Gomez LF, Kasi D, et al. [(18)F]T807, a novel tau positron emission tomography imaging agent for Alzheimer's disease. Alzheimers Dement 2013; 9: 666–76.